Pacific
Northwest
NATIONAL LABORATORY

Ceramic Waste Form Process for Immobilizing Iodine in Glass-Bonded Iodosodalite

September 2019

BJ Riley   NL Canfield
JA Peterson   SM Frank (INL)

U.S. DEPARTMENT OF
ENERGY

Ceramic Waste Form Process for Immobilizing Iodine in Glass-Bonded Iodosodalite

September 2019

BJ Riley   NL Canfield
JA Peterson   SM Frank (INL)

Abstract

A modified glass-bonded sodalite advanced ceramic waste form (ACWF) approach was used to fabricate ACWF-NaI or ACWF-AgI iodosodalite [i.e., $Na_8(AlSiO_4)_6I_2$] waste forms by occluding either NaI or AgI, respectively, into zeolite 4A at elevated temperatures, adding NBS-4 glass binder, and firing at 925°C. The phase purity of ACWF-NaI was 82.6 mass% $Na_8(AlSiO_4)_6I_2$ (with amorphous remainder) while the ACWF-AgI only had 25.9 mass% $Na_8(AlSiO_4)_6I_2$, despite the iodine being added as AgI; the remainder phases for ACWF-AgI included $NaAlSiO_4$ (15.1 mass%), AgI (4.5 mass%), and Ag^0 (0.2 mass%). This study shows that, starting from two different iodine salts, that the CWF process could be used for iodine immobilization.

Acknowledgments

Acronyms and Abbreviations

ACWF	advanced ceramic waste form
AgA	silver-exchanged Type-A zeolite
AgI	silver iodide
AgX	silver-exchanged faujasite
AgZ	silver-exchanged mordenite
CTE	coefficient of thermal expansion
CWF	ceramic waste form
EDS	energy dispersive spectroscopy
EtOH	ethanol
GBS	glass-bonded sodalite
GCM	glass-composite material
ICSD	Inorganic Crystal Structure Database
PNNL	Pacific Northwest National Laboratory
PXRD	powder X-ray diffraction
SEM	scanning electron microscopy
SG	space group
SOZ	salt occluded zeolite
WC	tungsten carbide
XRD	X-ray diffractometer

Contents

Figures

Tables

1.0 Introduction

Iodine is one of the more problematic species of interest when considering nuclear waste processing and immobilization strategies. In part, this is due to the inherent high volatility and low retention of iodine compounds during traditional melt-processing or sintering (Hrma, 2010) making it difficult to immobilize iodine in traditional borosilicate glasses (Riley et al., 2016), the most common waste form of choice for high-level wastes. These issues are compounded by the fact iodine is highly mobile in the environment, it is readily absorbed into the human metabolic system, and the half-life ($t_{1/2}$) of ^{129}I is 1.6×10^7 y so the waste form option chosen has to remain stable for millions of years.

Of the options that have been evaluated for iodine immobilization, only a few have shown promise to meet the criteria of high waste loading, high chemical durability, and low processing costs. Some of these options include iodosodalite (Babad and Strachan, 1980; Chong et al., 2017a), iodoapatite (Campayo et al., 2011; Cao et al., 2017), silver-functionalized silica aerogel (Matyáš et al., 2018; Matyáš et al., 2012), AgI immobilized in a glass (Yang et al., 2014), as well as iodine-loaded silver-zeolites (e.g., mordenite) either hot pressed into a monolithic waste form (Bruffey et al., 2017) or encapsulated in a glass matrix (i.e., a glass-composite material or GCM) (Nenoff et al., 2015).

The focus of the current work was to evaluate the incorporation of iodine as either NaI or AgI into iodosodalite using a modification of the baseline ceramic waste (CWF) process with more optimized glass binders than those used in previous experiments during the development of the process at Argonne National Laboratory (Ackerman et al., 1997; Bateman et al., 2007; Goff et al., 1996; Moschetti et al., 2000); the process is referred to as the advanced ceramic waste form (ACWF) process (Ebert and Snyder, 2015; Riley et al., 2017b). The NaI product can be generated through a variety of different approaches including Mercurex (Collard et al., 1980), Iodox (Holladay, 1979), electrolytic (Horner et al., 1977), caustic (Trevorrow et al., 1983), or molten hydroxide (Riley et al., 2018) processes, which are outlined elsewhere in more detail (Riley et al., 2016). Acquiring AgI is as simple as exposing the gaseous iodine [i.e., $I_{2(g)}$] to Ag (in the form of Ag^+ or Ag^0) and this can be done with Ag-loaded materials such as aerogels (Matyáš et al., 2018; Riley et al., 2017a) or zeolites such as mordenite (AgZ) (Jubin, 1981; Jubin et al., 2014) and faujasite (AgX) (Puppe and Wilhelm, 1989). Also, it is possible to acquire NaI by reacting iodine-loaded AgZ or AgX in an aqueous solution of Na_2S to generate NaI in solution whereas the Ag in the zeolite is converted to Ag_2S through Reaction (1) (Westphal et al., 2006) (ΔG is provided for 1 mole of $AgI_{(s)}$); note that the Ag_2S is very insoluble in aqueous solutions with a solubility product constant, $K_{sp} = 6.3 \times 10^{-50}$ (Zeng et al., 2018):

$$2\ AgI_{(s)} + Na_2S_{(ia)} \rightarrow 2\ NaI_{(a)} + Ag_2S_{(s)} \quad \Delta G = \text{-38.492 kJ mol}^{-1}\ (25°C) \tag{1}$$
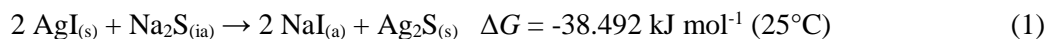
This work is similar to previous work by Maddrell et al. (2015), but with different precursors and without hot pressing where the target crystalline material was sodalite. Sodalite is of the cubic $P\bar{4}3n$ (218) [or less commonly $I\bar{4}3m$ (217)] space group and has the general formula of $R^I_8(R^{III}R^{IV}O_4)_6A_n$. Sodalite chemistry can vary within this construct, where the R^I cations balance the negative charge of the framework and are generally 1+ (e.g., K^+, Na^+), the R^{III} and R^{IV} components denote 3+ and 4+ cations, respectively (e.g., Al^{3+}, Ge^{4+}, Si^{4+}), and the A_n component is mostly represented by a variety of 1- anions (e.g., Cl^-, I^-, OH^-) (Lepry et al., 2013). In the most generic representation of the process described herein, NaI or AgI was occluded into zeolite 4A at elevated temperatures (i.e., 600–670°C), a glass binder was mixed in, and the mixture was heat-treated at 925°C to generate a glass-bonded iodosodalite waste form [i.e., glass-bonded $Na_8(AlSiO_4)_6I_2$]. This was done for NaI and AgI with targeted Reactions (2) and (3), respectively, while keeping the mass loading of glass binder fixed for both at 26 mass%.

$$Na_{12}(AlSiO_4)_{12} + 4\ NaI \rightarrow 2\ Na_8(AlSiO_4)_6I_2 \tag{2}$$

$$Na_{12}(AlSiO_4)_{12} + 4\,AgI \rightarrow 2\,Na_6Ag_2(AlSiO_4)_6I_2 \tag{3}$$

The generation of AgI-sodalite [i.e., $Ag_8(AlSiO_4)_6I_2$, $a = 0.89523$ nm] (Stein et al., 1992), absent of alkalis, was supported in the work by Maddrell et al. (2015), Stein et al. (1992), and Bruffey et al. (2016). Also, it is well known that the NaI-sodalite [i.e., $Na_8(AlSiO_4)_6I_2$, $a = 0.9008$ nm] (Stein et al., 1992) can be formed under a variety of conditions (Chong et al., 2017b; Maddrell et al., 2014; Stein et al., 1992; Strachan and Babad, 1979). However, while forming iodosodalite with a mixed Ag-alkali matrix has proven to be problematic (Maddrell et al., 2015), it has been documented in work by Stein et al. (1992) for a range of Na-Ag bromosodalites [$Na_{4-n}Ag_n(AlSiO_4)_6Br_2$], e.g., $Na_{7.7}Ag_{0.3}(AlSiO_4)_6Br_2$ ($a = 0.89290$ nm) and $Na_{5.5}Ag_{2.5}(AlSiO_4)_6Br_2$ ($a = 0.89123$ nm), and thus, might be possible.

2.0   Experimental Methods

2.1   Glass binder fabrication

The glass binder used in this study (NBS-4) is described elsewhere (Riley et al., 2017b) in more detail but a summary of how that glass was made along with some of the properties of the glass are provided here – see Table 1. The NBS-4 binder glass was fabricated by mixing appropriate amounts of 99+% pure oxides (i.e., SiO_2 and ZrO_2, carbonates (i.e., Na_2CO_3, $CaCO_3$), $Al(OH)_3$, and H_3BO_3 together in an agate milling chamber (Table 1). The mixture was melted in a Pt/10%Rh crucible with a lid for 30 minutes at 1550°C for 30 min and then poured onto an Inconel® quench plate. This glass was crushed in a tungsten carbide (WC) milling chamber, 0.5 mass% of Na_2SO_4 was added as a fining agent, this was mixed again in the WC milling chamber, and then this was melted at 1550°C for another 30 min. Then, a portion of the melt was casted into a steel mold and annealed while the rest was quenched on the Inconel plate. The quenched glass was carefully milled and a size fraction of (74–250 µm or -60/+200 mesh) was collected using sieves; this collected fraction was used to fabricate the waste forms described herein.

Table 1. Composition of NBS-4 glass binder along with measured properties from Riley et al. (2017b) with experimental error shown in parenthesis.

Composition		Properties	
Oxide	*Mass%*	*Parameter*	*Value*
SiO_2	58.87	T_M[a]	1550 (5) °C
Na_2O	20.17	T_g[b]	543.1 (0.3) °C
B_2O_3	8.98	T_s[c]	582.8 (4.0) °C
Al_2O_3	5.99	$\rho_{b,p}$[d]	2.5247 (0.0017) $\times 10^3$ kg m^{-3}
CaO	3.99	CTE-1[e]	10.99 (0.32) $\times 10^{-6}$ K^{-1}
ZrO_2	2.00	CTE-2[f]	72.46 (3.79) $\times 10^{-6}$ K^{-1}
SUM	100.00		

[a]Melting temperature (T_M)
[b]Glass transition temperature (T_g)
[c]Glass softening temperature (T_s)
[d]Bulk pycnometric density ($\rho_{b,p}$)
[e]Coefficient of thermal expansion (CTE) in region 1 ($T < T_g$)
[f]Coefficient of thermal expansion in region 2 ($T_g < T < T_s$)

2.2   ACWF fabrication

For both ACWF materials produced in this study, the general process was the same with specific details provided for each in Table 2. For each sample, processing and handling of the materials was conducted in an argon atmosphere glovebox. Specific masses (see Table 2) of zeolite 4A (i.e., 74–250 µm or -60/+200 mesh) and salts were mixed with mortar and pestle and transferred to an Al_2O_3 crucible and then placed in a muffle furnace for 24 hrs to occlude the salt into the zeolite (see Table 2 for more details). Four times during the heat treatment, the mixture was removed from the furnace and remixed in the mortar and pestle while still hot to help facilitate occlusion. Following this process, NBS-4 glass was added to the occluded zeolite with a target of ~26 mass% loading in the final mixture, and these were mechanically mixed then transferred into a glassy carbon crucible and placed in the muffle furnace at 925°C for 24 hrs. The final products were cooled to room temperature and then characterized using the procedures described below.

Table 2. Summary of experimental parameters for ACWF-NaI and ACWF-AgI fabrication.

Parameter	ACWF-NaI	ACWF-AgI
Salt mass (g)	6.5071 (NaI)	8.8003 (AgI)
Zeolite 4A mass (g)	18.4962	16.1230
Salt (mmoles)	21.7	18.7
Zeolite 4A (mmoles)	21.7	18.9
Salt:zeolite (molar)	1.000	0.991
SOZ (g)	24.6036	14.8827
SOZ:NBS-4 (by mass)[a]	2.84	2.84
Glass loading (mass%)	26.02	26.04
Salt loading (mass%)	19.25	26.12
Occlusion temperature (°C)	665	600

[a]SOZ denotes salt-occluded zeolite

2.3 Powder X-ray diffraction

Powder X-ray diffraction (PXRD) was conducted on both samples using a Bruker® D8 Advance (Bruker AXS Inc., Madison, WI) XRD with Cu K_α emission. The detector used was a LynxEye™ position-sensitive detector with a collection window of 3° 2θ. Scan parameters were 5–70° 2θ with a step of 0.015° 2θ and a 0.3-s dwell at each step. Bruker AXS DIFFRAC^{plus} EVA and AXS Topas (v4.2) were used to identify and quantify phase assemblages, respectively. So that the amorphous content could be quantified, ~5 mass% of a TiO_2 (rutile) standard (SRM-674b, 2018) was mixed into the sample prior to analysis.

2.4 Scanning electron microscopy and energy dispersive spectroscopy

Samples were mounted in resin and cross-section polished using glycol-based diamond suspensions down to 50-nm colloidal silica. Scanning electron microscopy (SEM) was performed with a JSM-7001F field-emission gun microscope (JEOL USA, Inc.; Peabody, MA) and energy dispersive spectroscopy (EDS) was performed using a Bruker xFlash 6|60 (Bruker AXS Inc., Madison, WI) spectrometer. EDS dot maps were collected at 50–100 k counts per second for about 30 minutes each. Bruker ESPRIT (v2) software was used to collect the data.

2.5 Density and porosity

2.5.1 Pycnometry

The bulk pycnometric densities, $\rho_{b,p}$. for each specimen were measured using a He pycnometer (Micromeritics AccuPyc II 1340, Norcross, GA) through a series of 5 purges and 10 measurements that were averaged. Mass values were measured with an XPE205 analytical balance (Mettler Toledo) and then the pycnometer calculated the average bulk pycnometric density, i.e., $\rho_{b,p} = m\ V^{-1}$ (kg m^{-3}).

2.5.2 Archimedes' technique

Archimedes' approach was used to assess the porosity and density of the CWF and ACWF specimens. Here, the specimen masses were measured dry (m_{dry}) on either a ME204E (Mettler Toledo) or AP310 (Ohaus Corporation, Parsippany, NJ) analytical balance and then submerged in absolute ethanol

(EtOH) within a vacuum desiccator where the air was removed from the open porosity and these voids were back-filled with absolute EtOH. After at least 20 min of sitting in the ethanol under vacuum (1.3–6.7 Pa), the submerged mass (m_{sub}) was measured using an Archimedes density kit (ME-DNY-4) from Mettler Toledo. Then, the pellet was removed from the EtOH and the excess EtOH on the surface of the pellet was removed by blotting it on an EtOH-soaked cloth, and the pellet saturated with EtOH was weighed (m_{sat}). The temperature of the EtOH was monitored and used to calculate the bulk Archimedes' density ($\rho_{b,A}$) of the pellet according to Equation (4) where the ρ_{EtOH} was the density of ethanol ($\rho_{EtOH} = -8.54\times10^{-4}*T + 0.806$; $T = 15$–25 °C (1924)). From these data, the open porosity (ϕ_A) of the specimens was measured based on mass differences as seen in Equation (5) (Lacks and Gordon, 1993). Finally, using the measured ϕ_A values, the theoretical sample volume was used in conjunction with the $\rho_{b,A}$ values to calculate the theoretical bulk Archimedes' densities ($\rho_{b,A(t)}$) correcting for the open porosity, while assuming no closed porosity, with Equation (6).

$$\rho_{b,A} = (m_{dry} * \rho_{EtOH}) / (m_{sat} - m_{sub}) \tag{4}$$

$$\phi_A = (m_{sat} - m_{dry}) / (m_{sat} - m_{sub}) \tag{5}$$

$$\rho_{b,A(t)} = \rho_{b,A} / (1 - \phi_A) \tag{6}$$

3.0 Results

3.1 Microstructure and chemistry (SEM-EDS)

The microstructures of the ACWF-NaI and ACWF-AgI waste forms can be found in Figure 1 and Figure 2, respectively, along with the corresponding EDS elemental dot maps for Si, Al, Na, I, and O (as well as Ag for ACWF-AgI). The sodalite grain can be distinguished from the glassy matrix by the distinct difference in contrast between the two phases where the iodine-containing sodalite is much brighter due to a notably higher average atomic number than the matrix glass phase, which appears black. The elemental distributions show stark differences for all of the elements tracked, except for oxygen. Spot EDS data for the glassy and sodalite regions within both ACWF-NaI and ACWF-AgI are shown in Table 3. While Si, Al, Na, and O are in both the glass and sodalite phases, it is evident that only Si is most abundant in the glassy matrix for ACWF-NaI. This is because the concentration of SiO_2 in NBS-4 is very high at ~59 mass%. For the ACWF-AgI sample, Si appears to be more concentrated in the glass.
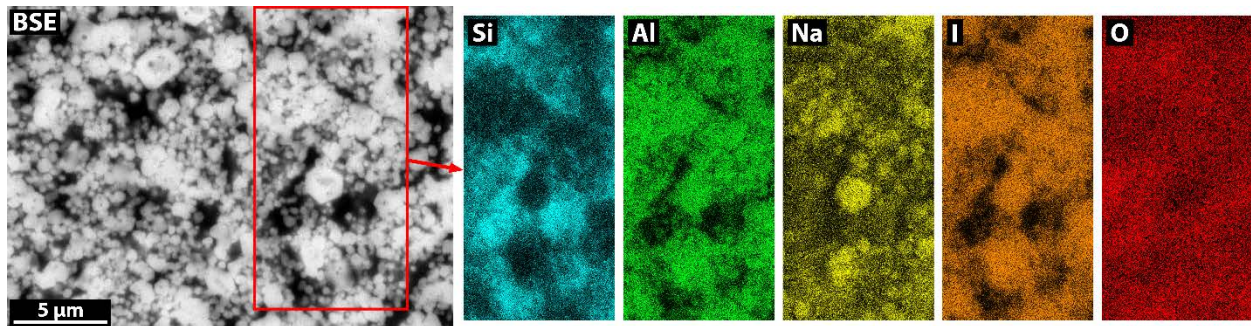
Figure 1. SEM-EDS for ACWF-NaI. The highlighted region in the BSE-SEM micrograph is the region where EDS dot mapping was performed.

Table 3. Summary of EDS compositions (atomic%, oxygen excluded) for ACWF-NaI and ACWF-AgI for both sodalite and glassy regions in each. Standard deviations are shown in parenthesis for each measurement.

Sample	Phase	Na	Al	Si	Ca	Zr	Ag	I
ACWF-NaI	Sodalite	34.5 (0.3)	22.3 (1)	35.8 (1.9)	1.3 (0.2)	0.1 (0.3)	- -	5.9 (0.7)
	Glass	33.2 (0.1)	13.7 (0.8)	47.6 (1.1)	3.3 (0.3)	1.8 (0.1)	- -	0.4 (0.5)
ACWF-AgI	Sodalite	25.8 (0.7)	20.1 (0.5)	45.8 (1.7)	0.1 (0.1)	0.9 (0.1)	0.01 (0.02)	7.3 (1.2)
	Glass	21.5 (0.2)	8.6 (0.4)	65.6 (0.3)	2.4 (0.1)	1.7 (0.2)	0.002 (0.002)	0.1 (0.1)
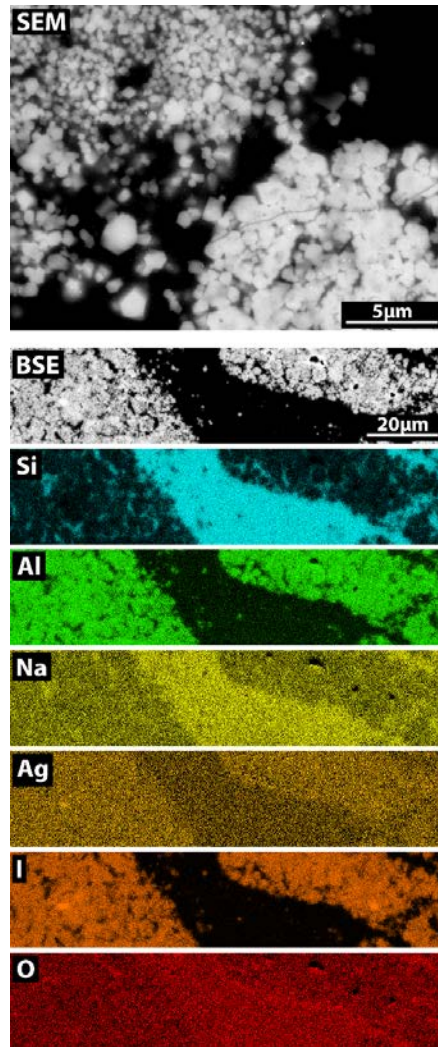
Figure 2. SEM-EDS results for ACWF-AgI.

The SEM-EDS analysis for both ACWF-NaI and ACWF-AgI showed that the sodalite phase for both samples were comprised of Na, Al, Si, O, and I; the sodalite for the ACWF-AgI sample showed a very low concentration of Ag present overall, but the Ag detected with EDS was shown to be concentrated in the sodalite phase (Table 3). A range of AgI crystals (verified with EDS) of different sizes were observed throughout the sample – see Figure 3 for an example of this. The Ag distribution in ACWF-AgI provides evidence of ion exchange between the Na-containing NBS-4 binder glass to form $Na_8(AlSiO_4)_6I_2$ sodalite.
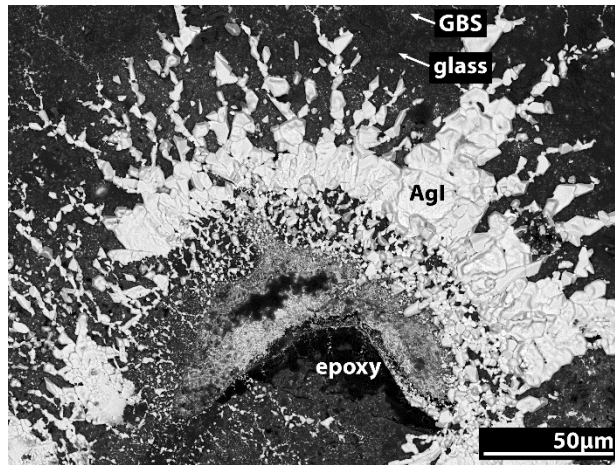
Figure 3. Appearance of AgI crystals (bright regions) present within the ACWF-AgI sample (dark regions at top of image). The glass-bonded sodalite (i.e., GBS), glass, AgI, and epoxy regions are labeled in the image.

3.2 Phase distribution (P-XRD)

The measured and calculated P-XRD patterns as well as difference spectra for ACWF-NaI and ACWF-AgI are shown in Figure 4 and Figure 5, respectively. The phase distribution for ACWF-NaI was highly crystalline $Na_8(AlSiO_4)_6I_2$ (82.6 mass%) with a sodalite unit cell parameter of $a = 0.90117$ nm, similar to values provided by Stein et al. ($a = 0.9008$ nm) (Stein et al., 1992) and Nielsen et al. (Nielsen et al., 1991a) ($a = 0.9009$ nm) – see Table 4.

The phase distribution for ACWF-AgI was more complex. This sample also had sodalite but it only consisted of 25.9 mass% of the total phase distribution. The unit cell parameter of the iodosodalite (0.90182 nm) was close to that of the iodosodalite found in ACWF-NaI (0.90117 nm, see above). The SEM-EDS analysis for both showed that both crystalline materials were comprised of Na, Al, Si, O, and I; the sodalite for the ACWF-AgI sample showed a very low concentration of Ag in the sodalite-rich regions. The vast majority of the Ag detected throughout the sample was present as AgI (i.e., 4.5 mass%) or Ag^0 (i.e., 0.2 mass%) as determined by P-XRD analysis (Figure 5). Other phases detected with P-XRD were $NaAlSiO_4$ (i.e., nepheline at 15.1 mass%) and an amorphous fraction of 54.3 mass%. The way that the AgI was distributed throughout the sample (see Figure 3), it was found at the boundaries of the glass-sodalite interface, suggesting that it was either pushed to the grain boundaries during crystallization of the sodalite phase during the heat-treatment process or remained agglomerated during the salt-occlusion process. It is also possible that the AgI is not stable at the sintering temperature and undergoes some phase transitions during that process.
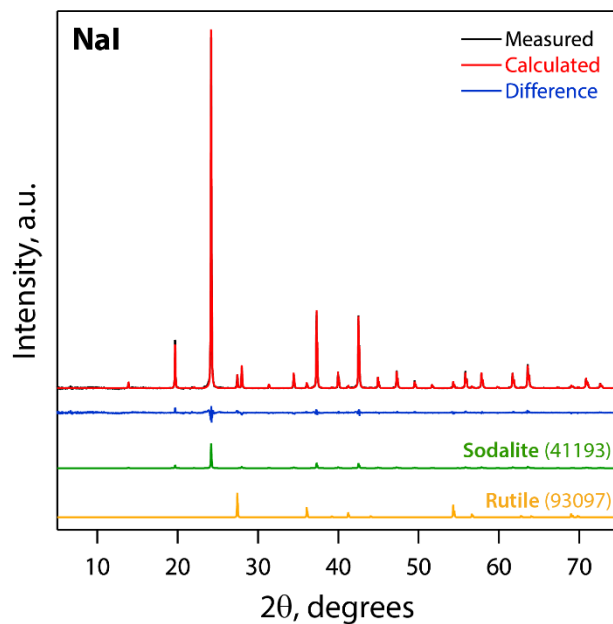
Figure 4. P-XRD pattern for ACWF-NaI showing the measured and calculated patterns as well as the difference spectrum.
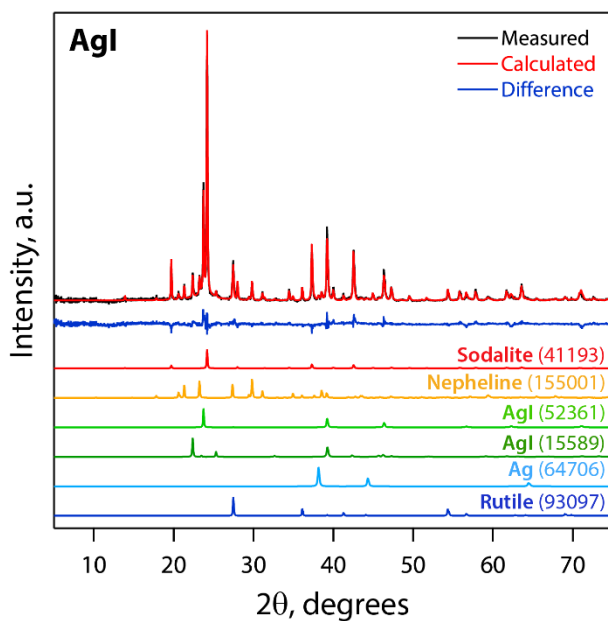
Figure 5. P-XRD pattern for ACWF-AgI showing the measured and calculated patterns as well as the difference spectrum.

3.4

Table 4. Summary of NaI, Ag-halide, and Ag-Na-halide sodalite crystals from the Inorganic Crystal Structure Database (ICSD; v1.9.5), if available, and the literature. The terms SG, a, V, and ρ_b denote space group, unit cell parameter, unit cell volume, and density, respectively.

Crystal chemistry	ICSD#	SG	a (nm)	V (nm³)	ρ_b (×10³ kg m⁻³)	Reference
$Na_8(AlSiO_4)_6I_2$	68960	$P\bar{4}3n$	0.90318	0.73675	2.6	(Weller and Wong, 1989)
$Na_8(AlSiO_4)_6I_2$	71434	$P\bar{4}3n$	0.9009	0.73119	2.62	(Nielsen et al., 1991b)
$Na_8(AlSiO_4)_6I_2$	41193	$I\bar{4}3m$	0.9008	0.73095	2.62	(Beagley et al., 1982)
$Na_8(AlSiO_4)_6I_2$	41194	$I\bar{4}3m$	0.9008	0.73095	2.62	(Beagley et al., 1982)
$Na_{7.95}Ag_{0.05}(AlSiO_4)_6Br_2$	-	$P\bar{4}3n$	0.8943	-	-	(Stein et al., 1992)
$Na_{7.76}Ag_{0.24}(AlSiO_4)_6Br_2$	71950	$P\bar{4}3n$	0.89289(3)	0.71186	2.49	(Stein et al., 1992)
$Na_{7.31}Ag_{0.69}(AlSiO_4)_6Br_2$	-	$P\bar{4}3n$	0.8941	-	-	(Stein et al., 1992)
$Na_{6.73}Ag_{1.27}(AlSiO_4)_6Br_2$	-	$P\bar{4}3n$	0.8939	-	-	(Stein et al., 1992)
$Na_{5.97}Ag_{2.03}(AlSiO_4)_6Br_2$	-	$P\bar{4}3n$	0.8934	-	-	(Stein et al., 1992)
$Na_{5.6}Ag_{2.4}(AlSiO_4)_6Br_2$	71951	$P\bar{4}3n$	0.89123(3)	0.7079	2.94	(Stein et al., 1992)
$Na_{4.95}Ag_{3.05}(AlSiO_4)_6Br_2$	-	$P\bar{4}3n$	0.8923	-	-	(Stein et al., 1992)
$Na_{4.1}Ag_{3.9}(AlSiO_4)_6Br_2$	-	$P\bar{4}3n$	0.8930	-	-	(Stein et al., 1992)
$Na_{3.32}Ag_{4.68}(AlSiO_4)_6Br_2$	-	$P\bar{4}3n$	0.8919	-	-	(Stein et al., 1992)
$Na_{2.3}Ag_{5.7}(AlSiO_4)_6Br_2$	-	$P\bar{4}3n$	0.8925	-	-	(Stein et al., 1992)
$Ag_6(AlSiO_4)_6$	79473	$P\bar{4}3n$	0.9122	0.75905	2.98	(Behrens et al., 1995)
$Ag_6(AlSiO_4)_6$	79474	$P\bar{4}3n$	0.9142	0.76405	2.96	(Behrens et al., 1995)
$Ag_6(AlSiO_4)_6$	88554	$P\bar{4}3n$	0.91189	0.75828	2.98	(Latturner et al., 1999)
$Ag_8(AlSiO_4)_6Br_2$	-	$P\bar{4}3n$	0.8926	-	-	(Stein et al., 1992)

3.3 Porosity and density

The measured ϕ_A values for both ACWF-NaI and ACWF-AgI were notably high at 52 and 25 vol%, respectively (Table 5). These ϕ_A values are comparable to data gathered in a previous study for waste forms made using the same CWF process and the same NBS-4 binder glass, albeit with a different salt (Riley et al., 2017b). While not the focus of the current study, if a hot-pressing technique such as hot uniaxial pressing (HUP) or hot isostatic pressing (HIP) were used, the porosity of the final waste form fabricated using this process could be drastically reduced. Additionally, the porosity could be further reduced if (a) a higher mass loading of glass binder were used as demonstrated in a previous study (Riley et al., 2017b) and/or (b) if a lower salt loading were used.

The measured densities of the ACWF-NaI and ACWF-AgI were notably different at 2.55 and 2.71×10³ kg m⁻³ for $\rho_{b,p}$, respectively, and 2.57 and 2.71×10³ kg m⁻³ for $\rho_{b,A(t)}$, respectively. Note that the values of $\rho_{b,p}$ and $\rho_{b,A(t)}$ for each sample were very consistent, providing some confidence that the ϕ_A values were mostly comprised of open porosity.

Table 5. Summary of $\rho_{b,p}$, $\rho_{b,A}$, ϕ_A, and $\rho_{b,A(t)}$ values for ACWF-NaI and ACWF-AgI.

Sample	$\rho_{b,p}$ (×10³ kg m⁻³)	$\rho_{b,A}$ (×10³ kg m⁻³)	ϕ_A (vol%)	$\rho_{b,A(t)}$ (×10³ kg m⁻³)
ACWF-NaI	2.5487 (0.0032)	1.2302	52.2	2.5717
ACWF-AgI	2.7082 (0.0024)	2.0229	25.4	2.7113

4.0   Discussion

While the glass-bonded sodalite ceramic waste form process has been demonstrated for immobilizing chloride salts at an industrial scale (Priebe and Bateman, 2006), it has not been demonstrated at these scales for immobilizing iodine-rich salts. Previous work by Babad and Strachan (1980), Maddrell, et al. (Maddrell et al., 2014; Maddrell et al., 2015; Sheppard et al., 2006), Bruffey and Jubin et al. (Bruffey et al., 2017; Bruffey et al., 2016), Kroll et al. (2018), and Chong et al. (2017a) have shown that iodosodalite waste forms can be made relatively easily through a variety of syntheses processes including solid-state procedures (current work), sol-gel procedures (Kroll et al., 2018), solution-based procedures (Babad and Strachan, 1980; Chong et al., 2017a; Maddrell et al., 2014), as well as loading Ag-exchanged zeolites (e.g., AgA or Ag-exchanged Type-A zeolite, AgX or Ag-exchanged faujasite) with iodine and hot pressing (Bruffey et al., 2017; Bruffey et al., 2016; Maddrell et al., 2015).

The most promising technology for large-scale processing is likely the pressure-less consolidation CWF process, which was used in the current work on a much smaller scale, because it is the most technologically mature and does not require the use of Ag. The CWF process has been demonstrated at industrial scales to make glass-bonded sodalite CWF waste forms that are up to 400 kg (Priebe and Bateman, 2006). However, the optimization of the glass binder for iodine-based salts has not yet been done. The current work demonstrates that, using zeolite 4A [i.e., $Na_{12}(AlSiO_4)_{12}$], the CWF process utilizing the NaI salt yielded single-phase glass-bonded $Na_8(AlSiO_4)_6I_2$ waste form, whereas using AgI, several other phases are present. It is not known which system is more preferred from a waste form standpoint being that the chemical durability of AgI, the unincorporated salt for ACWF-AgI, is still rather high ($K_{sp} = 8.5\times10^{-17}$–$9.3\times10^{-17}$ (Liu et al., 2015; Zeng et al., 2018)), but the current work shows that both approaches can be used to make Iodosodalite, albeit the NaI approach is more advantageous with less complex results. It was also observed that, even when the starting salt was AgI, the resulting iodosodalite was still of the $Na_8(AlSiO_4)_6I_2$ composition showing ion exchange between the starting salt (i.e., AgI) and the Na_2O contributed from the glass binder (i.e., NBS-4) as was documented using the CWF process for a mixed chloride salt simulant in a previous study (Riley et al., 2017b).

5.0   Summary and Conclusions

The glass-bonded sodalite ceramic waste form process previously demonstrated at industrial scales for immobilizing spent EBR-II salt wastes was demonstrated on a small scale in the current studying by occluding either NaI (i.e., ACWF-NaI) or AgI (ACWF-AgI) into zeolite 4A at elevated temperatures (i.e., 600–700°C), adding in a high-Na_2O glass binder (i.e., NBS-4) at 26 mass%, and firing at 925°C. The ACWF-NaI waste form was a glass-bonded iodosodalite [i.e., 82.6 mass% $Na_8(AlSiO_4)_6I_2$ and 17.4 mass% amorphous] while the ACWF-AgI waste form had 25.9 mass% $Na_8(AlSiO_4)_6I_2$ but several other crystalline phases including 15.1 mass% nepheline, 4.5 mass% AgI, 0.2 mass% Ag^0, and a large amorphous fraction of 54.3 mass% amorphous material.

These results show promise that either NaI or AgI salts could be immobilized in glass-bonded sodalite using the CWF process, but the NaI is a much more attractive process from a simplicity perspective, and because it does not include Ag, which is both a precious metal and toxic to the environment. While the NaI process yielded a much higher phase purity of $Na_8(AlSiO_4)_6I_2$ than the AgI process, both processes yielded chemically durable crystalline phases that show promise for chemically durable waste forms. By considering the results from a previous study on CWF optimization (Riley et al., 2017b), additional improvements that could be made to optimize the final iodosodalite product include higher glass binder loadings, using a hot pressing technique to help with densification, and lower salt loadings.

6.0 References

Ackerman, J. P., L. S. H. Chow, S. M. McDeavitt, C. Pereira, and R. H. Woodman. 1997. "Isolating wastes in the electrometallurgical treatment of spent nuclear fuel." *Journal of The Minerals, Metals & Materials Society* **49**(7):26-28.

Babad, H. and D. M. Strachan. 1980. "Method for immobilizing radioactive iodine." US Patent No. 4229317.

Bateman, K. J., C. J. Knight, and C. W. Solbrig. 2007. *Current Status of Ceramic Waste Form Development*. INL/INT-06-11736, Rev. 1, Idaho National Laboratory, Idaho Falls, ID.

Beagley, B., C. M. B. Henderson, and D. Taylor. 1982. "The crystal structures of aluminosilicate-sodalites: X-ray diffraction studies and computer modelling." *Mineralogical magazine* **46**(341):459-64.

Behrens, P., P. B. Kempa, S. Assmann, M. Wiebcke, and J. Felsche. 1995. "The structures of anhydrous silver sodalite $Ag_3(Al_3Si_3O_{12})$ at 298, 623, and 723 K from Rietveld refinements of X-ray powder diffraction data: mechanism of thermal expansion and of the phase transition at 678 K." *Journal of Solid State Chemistry* **115**:55-65.

Bruffey, S. H., J. A. Jordan, R. T. Jubin, M. L. Parks, and T. R. Watkins. 2017. *Hot Isostatic Pressing of Engineered Forms of I-AgZ*. NTRD-MRWFD-2017-000412, ORNL/SR-2017/707, Oak Ridge National Laboratory, Oak Ridge, TN.

Bruffey, S. H., R. T. Jubin, and J. A. Jordan. 2016. *Fundamental Aspects of Zeolite Waste Form Production by Hot Isostatic Pressing*. FCRD-MRWFD-2016-000267, ORNL/SR-2016/759, Oak Ridge National Laboratory, Oak Ridge, TN.

Campayo, L., A. Grandjean, A. Coulon, R. Delorme, D. Vantelon, and D. Laurencin. 2011. "Incorporation of iodates into hydroxyapatites: a new approach for the confinement of radioactive iodine." *Journal of Materials Chemistry* **21**(44):17609-11.

Cao, C., S. Chong, L. Thirion, J. C. Mauro, J. S. McCloy, and A. Goel. 2017. "Wet chemical synthesis of apatite-based waste forms - A novel room temperature method for the immobilization of radioactive iodine." *Journal of Materials Chemistry A* **5**(27):14331-42.

Chong, S., J. Peterson, J. Nam, B. Riley, and J. McCloy. 2017a. "Synthesis and characterization of iodosodalite." *Journal of the American Ceramic Society* **100**(5):2273-84.

Chong, S., J. A. Peterson, J. Nam, B. J. Riley, and J. S. McCloy. 2017b. "Synthesis and characterization of iodosodalite." *J. Am. Ceram. Soc.*

Collard, G. E. R., D. Hennart, J. Van Dooren, and W. R. A. Goosens. 1980. Iodine trapping and conditioning in the Mercurex process. In *Proceedings of 16th DOE Nucl. Air Clean. Conf.* eds. MW First, pp. 552-64, United States Nuclear Regulatory Commission, Cambridge, MA.

Ebert, W. L. and C. T. Snyder. 2015. *Corrosion Tests with Waste Forms Developed for EChem Salt Wastes*. FCRD-MRWFD-2015-000145, Argonne National Laboratory, Lemont, IL.

Goff, K. M., R. W. Benedict, K. Bateman, M. A. Lewis, c. Pereira, and C. A. Musick. 1996. Spent fuel treatment and mineral waste form development at Argonne National Laboratory-West. Presented at

International Topical Meeting on Nuclear and Hazardous Waste Management. SPECTRUM '96, Vol. 3, pp. 2436-43, American Nuclear Society.

Hocdé, S., S. B. Jiang, X. Peng, N. Peyghambarian, T. Luo, and M. Morrell. 2004. "Er^{3+} doped boro-tellurite glasses for 1.5 µm broadband amplification." *Optical Materials* **25**(2):149-56.

Holladay, D. W. 1979. *A literature survey: methods for the removal of iodine species from off-gases and liquid waste streams of nuclear power and nuclear fuel reprocessing plants, with emphasis on solid sorbents*. ORNL/TM-6350, Oak Ridge National Laboratory, Oak Ridge, TN.

Horner, D. E., J. C. Mailen, and F. A. Posey. 1977. "Electrolytic trapping of iodine from process gas streams." United States Application No. 4004993.

Hrma, P. R. 2010. *Retention of Halogens in Waste Glass*. PNNL-19361, Pacific Northwest National Laboratory, Richland, WA.

Jubin, R. T. 1981. *Organic Iodine Removal from Simulated Dissolver off-Gas Systems Utilizing Silver-Exchanged Mordenite*. Oak Ridge National Laboratory, Oak Ridge, TN.

Jubin, R. T., S. H. Bruffey, and K. K. Patton. 2014. *Expanded Analysis of Hot Isostatic Pressed Iodine-Loaded Silver-Exchanged Mordenite*. FCRD-SWF-2014-000278, ORNL/LTR-2014/476, Oak Ridge National Laboratory, Oak Ridge, TN.

Kroll, J. O., B. J. Riley, J. S. McCloy, J. A. Peterson, and J. Matyáš. 2018. "Sol-gel synthesis and consolidation of iodosodalite." *for submittal to Journal of Nuclear Materials*.

Lacks, D. J. and R. G. Gordon. 1993. "Crystal-structure calculations with distorted ions." *Physical Review B* **48**(5):2889-908.

Latturner, S. E., J. Sachleben, B. B. Iversen, J. C. Hanson, and G. D. Stucky. 1999. "Covalent guest-framework interactions in heavy metal sodalites: structure and properties of thallium and silver sodalite." *Journal of Physical Chemistry B* **103**:7135-44.

Lepry, W. C., B. J. Riley, J. V. Crum, C. P. Rodriguez, and D. A. Pierce. 2013. "Solution-based approaches for making high-density sodalite waste forms to immobilize spent electrochemical salts." *Journal of Nuclear Materials* **442**(1–3):350-59.

Liu, Q., X. Hou, W. Zhou, and Y. Fu. 2015. "Accelerator mass spectrometry analysis of ultra-low-level ^{129}I in carrier-free AgI-AgCl sputter targets." *Journal of The American Society for Mass Spectrometry* **26**(5):725-33.

Maddrell, E., A. Gandy, and M. Stennett. 2014. "The durability of iodide sodalite." *Journal of Nuclear Materials* **449**(1–3):168-72.

Maddrell, E. R., E. R. Vance, and D. J. Gregg. 2015. "Capture of iodine from the vapour phase and immobilisation as sodalite." *Journal of Nuclear Materials* **467**:271-79.

Matyáš, J., E. S. Ilton, and L. Kovařík. 2018. "Silver-functionalized silica aerogel: towards an understanding of aging on iodine sorption performance." *RSC Advances* **8**(56):31843-52.

Matyáš, J., M. J. Robinson, and G. E. Fryxell. 2012. "The Effect of Temperature and Uniaxial Pressure on the Densification Behavior of Silica Aerogel Granules." In *Ceramic Materials for Energy Applications II*, eds. K Fox, et al., Vol 33, pp. 121-32. John Wiley & Sons, Inc.

Moschetti, T. L., W. Sinkler, T. DiSanto, M. H. Novy, A. R. Warren, D. Cummings, S. G. Johnson, K. M. Goff, K. J. Bateman, and S. M. Frank. 2000. Characterization of a ceramic waste form encapsulating radioactive electrorefiner salt. Presented at *Sci. Basis Nucl. Waste Mgt., XXIII*, pp. 577-82, Mat. Res. Soc., Pittsburgh, PA.

Nenoff, T. M., T. J. Garino, P. V. Brady, and C. D. Mowry. 2015. Low-temperature glass composite material (GCM) waste form for radiological iodine captured by Ag-zeolites: Optimization and durability (Paper 5054). In *Proceedings of Global 2015*.

Nielsen, N. C., H. Bildsøe, H. J. Jakobsen, and P. Norby. 1991a. "^{7}Li, ^{23}Na, and ^{27}Al quadrupolar interactions in some aluminosilicate sodalites from MAS n.m.r. spectra of satellite transitions." *Zeolites* **11**(6):622-32.

Nielsen, N. C., H. Bildsøe, H. J. Jakobsen, and P. Norby. 1991b. "^{7}Li, ^{23}Na, and ^{27}Al quadrupolar interactions in some aluminosilicate sodalites from MAS NMR spectra of satellite transitions." *Zeolites* **11**(6):622-32.

Priebe, S. and K. Bateman. 2006. "The ceramic waste form process at the Idaho National Laboratory." *Nuclear Technology* **162**(2):199-207.

Puppe, L. and J. Wilhelm. 1989. "Process for removal of iodine and iodine compounds from gases and vapours with silver containing zeolite X." Patent No. EP332964 A3.

Riley, B. J., J. O. Kroll, J. A. Peterson, J. Matyáš, M. J. Olszta, X. Li, and J. D. Vienna. 2017a. "Silver-Loaded Aluminosilicate Aerogels As Iodine Sorbents." *ACS Applied Materials & Interfaces* **9**(38):32907-19.

Riley, B. J., J. McFarlane, G. D. DelCul, J. D. Vienna, C. I. Contescu, L. M. Hay, A. V. Savino, and H. E. Adkins. 2018. *Identification of Potential Waste Processing and Waste Form Options for Molten Salt Reactors*. NTRD-MSR-2018-000379, PNNL-27723, Pacific Northwest National Laboratory, Richland, WA.

Riley, B. J., J. D. Vienna, S. M. Frank, J. O. Kroll, Z. Zhu, N. L. Canfield, K. Kruska, D. K. Schreiber, J. A. Peterson, and J. V. Crum. 2017b. "Glass Binder Development for a Glass-Bonded Sodalite Ceramic Waste Form." *J. Nucl. Mater.* **489**:42-63.

Riley, B. J., J. D. Vienna, D. M. Strachan, J. S. McCloy, and J. L. Jerden Jr. 2016. "Materials and processes for the effective capture and immobilization of radioiodine: A review." *Journal of Nuclear Materials* **470**:307-26.

Sheppard, G. P., J. A. Hriljac, E. R. Maddrell, and N. C. Hyatt. 2006. Silver zeolites: iodide occlusion and conversion to sodalite—A potential I-129 waste form? In *Proceedings of Scientific Basis for Nuclear Waste Management XXIX*. eds. P Van Iseghem, vol. 932, pp. 775–82, Materials Research Society, Warrendale, PA.

SRM-674b. 2018. X-Ray Powder Diffraction Intensity Set (Quantitative Powder Diffraction Standard), National Institute of Standards and Technology.

Stein, A., G. A. Ozin, P. M. Macdonald, G. D. Stucky, and R. Jelinek. 1992. "Silver, sodium halosodalites: class A sodalites." *Journal of the American Chemical Society* **114**(13):5171-86.

Strachan, D. M. and H. Babad. 1979. "Iodide and iodate sodalites for long-term storage of I-129." *American Ceramic Society Bulletin* **58**(3):327.

Stratton, S. W. 1924. *Standard density and volumetric tables*, 6th ed., United States National Bureau of Standards, Government Printing Office, Washington.

Trevorrow, L. E., G. F. Vandegrift, V. M. Kolba, and M. J. Steindler. 1983. *Compatibility of Technologies with regulations in the waste management of H-3, I-129, C-14, and Kr-85. Part I. Initial information base*. ANL-83-57, Argonne National Laboratory Argonne, IL.

Weller, M. T. and G. Wong. 1989. "Mixed halide sodalites." *Eur. J. Solid State Inorg. Chem.* **26**(6):619-33.

Westphal, B. R., J. J. Park, G. D. Del Cul, and K. J. Bateman. 2006. *Development of Voloxidation Process for Treatment of LWR Spent Fuel*. I-NERI Annual Technical Report, Project 2004-004-K, Idaho National Laboratory, Idaho Falls, ID.

Yang, J. H., J. M. Shin, J. J. Park, and G. I. Park. 2014. "Waste form of silver iodide (AgI) with low-temperature sintering glasses." *Separation Science and Technology* **49**(2):298-304.

Zeng, J., M. Li, A. Liu, F. Feng, T. Zeng, W. Duan, M. Li, M. Gong, C.-Y. Wen, and Y. Yin. 2018. "Au/AgI dimeric nanoparticles for highly selective and sensitive colorimetric detection of hydrogen sulfide." *Advanced Functional Materials* **28**(26):1800515, doi: 10.1002/adfm.201800515.